Photocatalysis

DOI: 10.1002/anie.201206817

Triazine-based Carbon Nitrides for Visible-Light-Driven Hydrogen Evolution**

*Katharina Schwinghammer, Brian Tuffy, Maria B. Mesch, Eva Wirnhier, Charlotte Martineau, Francis Taulelle, Wolfgang Schnick, Jürgen Senker, and Bettina V. Lotsch**

The development of catalysts that enable the direct conversion of solar energy into chemical energy has been defined as one of the major challenges of modern materials chemistry. Hydrogen generated by photochemical water splitting has been identified as a promising energy carrier that offers a high energy density while being environmentally clean.[1] Nevertheless, to realize a light-driven hydrogen-based economy, the exploration of new materials for highly efficient, stable, economically viable, and environmentally friendly photocatalysts is required.

To date, numerous inorganic semiconductors have been developed for water splitting, most of them being transition metal compounds containing heavy metals such as La, Bi, Ta, or Nb, which impede scalability, increase cost, and add complexity.[2] Recently, attention has been attracted to a new class of metal-free photocatalysts, comprising polymeric melon-type carbon nitrides (CNs) based on imide-bridged heptazine units (see Figure 1 a).[3] CNs are readily accessible, lightweight, stable, and low-cost compounds that offer an attractive alternative to metal-rich catalysts while still maintaining efficient photoactivity.[4] Thermal condensation of CNs forms a wide variety of chemical species that differ substantially with respect to their degree of condensation, hydrogen content, crystallinity, and morphology.[5,6] The chemical modification of CNs by molecular "dopants" has resulted in a number of CN materials with improved photocatalytic activity.[7] Although the evidence is largely empirical, the property enhancement presumably originates from subtle modifications of the parent structures by incorporation of heteroatoms as well as structural defects, to give rise to enhanced absorption in the visible light range and a more complete exploitation of the solar energy spectrum.

In contrast to all known CN photocatalysts, which are composed of heptazine building blocks, poly(triazine imide) (PTI/Li^+Cl^-) is the only structurally characterized 2D CN network featuring imide-linked triazine units (see Figure 1 b).[8,9] Owing to its high level of crystallinity, PTI/Li^+Cl^- lends itself as an excellent model system to study photocatalytic activity towards water splitting as a function of the number of building blocks, the composition, and the degree of structural perfection of the system. Herein, we present a new generation of CN photocatalysts based on triazine building blocks and demonstrate their enhanced photocatalytic activity in comparison to heptazine-based CNs. Moreover, we show that their performance can be amplified by small-molecule doping, thus rendering them the most active nonmetal photocatalysts for the hydrogen evolution reaction that have been reported to date.

As a starting point, we synthesized crystalline PTI/Li^+Cl^- as a model structure for triazine-based CNs in a two-step ionothermal synthesis according to the procedure of Wirnhier et al.[8,9] To study the effect of crystallinity on the photocatalytic activity, we also synthesized an amorphous variant of PTI (aPTI), through a one-step ionothermal synthesis involving a LiCl/KCl salt melt. We used 4-amino-2,6-dihydroxypyrimidine (4AP; Figure 1 d) as the dopant because of its structural similarity to melamine and higher carbon and oxygen content. The photocatalytic activity of the as-prepared CNs was compared with that of crystalline PTI/Li^+Cl^- and of heptazine-based raw melon (see the Supporting Information).

The XRD patterns of the aPTI samples confirm their amorphous character by the absence of sharp reflections (see the Supporting Information, Figure S1), which are present in the XRD patterns of crystalline PTI/Li^+Cl^-. However, the FTIR spectra of the synthesized aPTI CNs are still largely similar to that of PTI/Li^+Cl^-[8] (Figure 2 d and Figures S2–5 in the Supporting Information), as they contain a band at 810 cm^{-1} (ring sextant out of plane bending) and a fingerprint region between 1200 and 1620 cm^{-1} that is dominated by ν(C–NH–C) and ν(C=N) stretching vibrations.[5,10] Doping with 4AP gives rise to less well-defined IR bands, thereby indicating a decrease in the structural order. In addition, in the spectra of 16% and 32% doped PTI there is a band at 914 cm^{-1} that can be assigned to aromatic C–H bending vibrations of the dopant (see the Supporting Information,

[*] K. Schwinghammer, B. Tuffy, Prof. B. V. Lotsch
Max Planck Institute for Solid State Research
Heisenbergstr. 1, 70569 Stuttgart (Germany)
E-mail: B.Lotsch@fkf.mpg.de
Homepage: http://www.cup.uni-muenchen.de/ac/lotsch/
K. Schwinghammer, B. Tuffy, E. Wirnhier, Prof. W. Schnick, Prof. B. V. Lotsch
Department of Chemistry, University of Munich, LMU
Butenandtstr. 5–13, 81377 Munich (Germany)
M. B. Mesch, Prof. J. Senker
Department of Inorganic Chemistry III, University of Bayreuth
Universitätsstr. 30, 95447 Bayreuth (Germany)
C. Martineau, Prof. F. Taulelle
Tectospin, Institut Lavoisier de Versailles (ILV), UMR CNRS 8180
Université de Versailles Saint-Quentin-en-Yvelines
45 Avenue des Etats-Unis, 78035 Versailles cedex (France)

[**] Financial support by the Deutsche Forschungsgemeinschaft (projects LO1801/1-1, SCHN377/15-1, SE1417/5-1), the cluster of excellence "Nanosystems Initiative Munich" (NIM), and the Center for NanoScience (CeNS) is gratefully acknowledged. We thank V. Duppel, C. Minke, A. Ranft, S. Hug, M. Schreiber, and W. König for their assistance with the experimental work.

Supporting information for this article is available on the WWW under http://dx.doi.org/10.1002/anie.201206817.

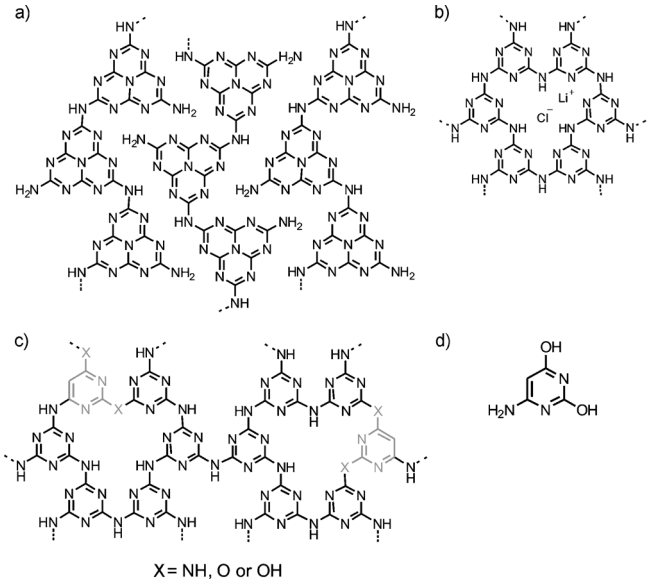

Figure 1. Chemical structures of a) melon, b) PTI/Li^+Cl^- (idealized structure), c) aPTI_4AP$_{16\%}$ (proposed structure), and d) the dopant 4AP.

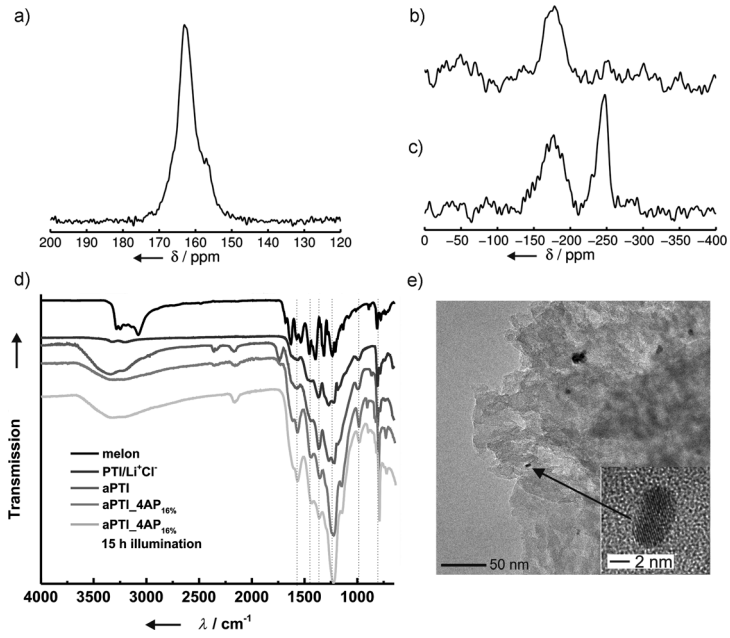

Figure 2. a) ^{13}C CP–MAS NMR spectrum (10 kHz), b) ^{15}N CPPI MAS NMR spectrum (6 kHz, inversion time = 400 μs) and c) ^{15}N CP–MAS NMR spectrum (10 kHz) of aPTI_4AP$_{16\%}$. d) FTIR spectra of aPTI_4AP$_{16\%}$ synthesized at 550 °C before and after 15 h illumination, compared to crystalline PTI/Li^+Cl^-, aPTI$_{500°C}$, and melon. e) A typical image of 2.3 wt% Pt-loaded aPTI_4AP$_{8\%}$ after illumination for 3 h under visible light ($\lambda > 420$ nm) and at higher magnification (inset).

Figure S5). Interestingly, the bands at 2160 cm^{-1}, 1730 cm^{-1}, and around 1200 cm^{-1}, which are seen in the spectrum of aPTI and partially in those of the doped samples, point to the presence of terminal nitrile groups as well as oxygen-containing functionalities, such as C=O and C–O.

Elemental analysis (EA) indicates the atomic ratio C/N = 0.68 for PTI/Li^+Cl^-, whereas the C/N ratios of the aPTI samples are slightly increased for those synthesized at elevated temperatures, indicating either a higher degree of condensation or an increase of oxygen incorporation (see the Supporting Information, Table S1). Notably, the amount of Li and Cl is lower in doped and nondoped aPTI than in crystalline PTI/Li^+Cl^-, whereas the oxygen content is significantly higher, consistent with the IR results. This finding is worth noting as the amount of carbon and oxygen atoms in CNs is likely to play an essential role in the activity of CN photocatalysts.[11] By increasing the amount of 4AP incorporated in the doped PTI from 2% to 64% the C/N ratio increases from 0.69 to 1.13, respectively (see the Supporting Information, Table S2). In summary, the EA and IR results suggest that both carbon and oxygen atoms are incorporated into the amorphous materials, most likely through replacement of one of the ring or bridging nitrogen atoms, as proposed in Figure 1c.

The ^{13}C and ^{15}N cross-polarization magic-angle spinning (CP–MAS) NMR spectra (Figure 2a and c) for aPTI doped with 16% 4AP and synthesized at 550 °C (aPTI_4AP$_{16\%}$) provide additional information about the structural composition of the material derived from copolymerization with 4AP. Both spectra are similar to those of PTI/Li^+Cl^- (see the Supporting Information, Figure S6),[8,9] albeit with significantly increased line width (full width at half maximum (FWHM)) of 1.5 kHz compared to 600 Hz) owing to the less ordered character of the materials (see the Supporting Information, Figure S1). The ^{15}N CP–MAS spectrum shows two broad signal groups centered around −175 and −245 ppm. The former group is typical for tertiary ring nitrogen atoms (N_{tert}; from the outer ring nitrogen atoms of heptazine or triazine rings), whereas the latter is characteristic of bridging NH groups. A very weak signal around −280 ppm indicates that only a small amount of terminal NH_2 groups is present, hence a melon-type structure seems very unlikely. However, to further corroborate this hypothesis and identify the type of heterocycle formed under the conditions used—triazine versus heptazine—we recorded a ^{15}N cross polarization polarization inversion (CPPI)[12] NMR spectrum of aPTI_4AP$_{16\%}$ (Figure 2b) with an inversion time of 400 μs. Under such conditions, resonances of the NH groups are reduced to zero intensity whereas signals of NH_2 units will be inverted. In contrast, the ^{15}N signals of tertiary nitrogen atoms are expected to remain largely unaffected. Hence, the unique signal for the central nitrogen atom, N_c, of a heptazine ring between -220 and -240 ppm can unequivocally be identified.[5] The absence of any signals in the ^{15}N CPPI spectrum (Figure 2b) in the region between −200 and −300 ppm therefore strongly suggests the absence of heptazine units within the detection limit of roughly 10–15%. The markedly different intensity ratios in the ^{13}C CP–MAS spectrum of aPTI_4AP$_{16\%}$ (Figure 2a) compared to those in the ^{13}C CP–MAS spectrum of PTI/Li^+Cl^-, and the broad asymmetric high-field flank of the signal between −140 and −170 ppm in the ^{15}N CP–MAS spectrum (Figure 2c) may indicate partial incorporation of

pyrimidine into the PTI framework during copolymerization, which is not observed for PTI/Li^+Cl^-.[8,9]

The brown color of crystalline PTI/Li^+Cl^- indicates substantial absorption in the visible range of the spectrum. More specifically, the material absorbs largely in the UV region, yet additional absorption takes place in the blue part of the visible region and there is a gradual decrease in absorption toward higher wavelengths (Figure 3 and Figure S7 in the Supporting Information). The absorption spectra of aPTI synthesized at 400–600 °C show bands that are comparable to those in the spectrum of melon, thus rendering the color of the materials similar to that of melon (see the Supporting Information, Figures S7 and S10). When the reaction temperature is increased, the color of aPTI changes from cream (400 °C) to yellow (500 °C), suggesting enhanced absorption in the visible region. The absorption of $aPTI_{500°C}$, which is synthesized at a reaction temperature of 500 °C, is strongly red-shifted compared to that of crystalline PTI/Li^+Cl^-, thereby representing further improvement in the visible-light absorption (see the Supporting Information, Figure S7 (1)). With increasing amounts of dopant the color of the 4AP-doped CNs gets darker, changing from yellow (2%) to red-brown (64%); this color change correlates well with the red-shift observed in the absorption spectra (see the Supporting Information, Figure S8).

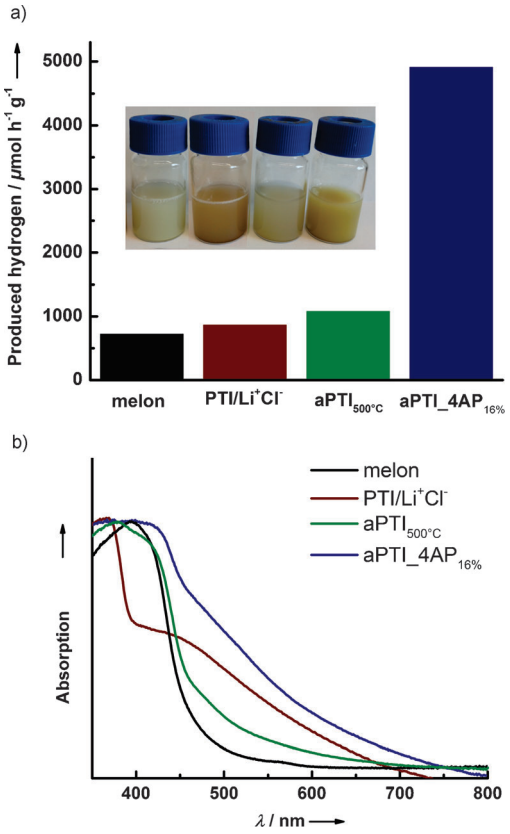

Figure 3. Photocatalytic activity towards hydrogen production (a). UV–Vis spectra (b) and color of the water/TEoA suspensions (inset in a) of $aPTI\_4AP_{16\%}$ synthesized at 550 °C compared to crystalline PTI/Li^+Cl^-, aPTI synthesized at 500 °C, and melon.

The inherent 2D architecture of crystalline PTI/Li^+Cl^- gives rise to an expanded π-electron system, lower band-gap, and enhanced absorption as compared to the 1D polymer melon, and thus renders PTI/Li^+Cl^- a promising photocatalyst that may even outperform the heptazine-based semiconductors. In fact, hydrogen production of 864 $\mu mol\,h^{-1}\,g^{-1}$ (ca. 15% error) was measured for crystalline PTI/Li^+Cl^- in the presence of a Pt co-catalyst and triethanolamine (TEoA) as sacrificial electron donor; this result equates to an enhancement of approximately 20% compared to synthesized raw melon (see the Experimental Section; 722 $\mu mol\,h^{-1}\,g^{-1}$) and is comparable to "g-C_3N_4" synthesized at 600 °C (synthesis according to Zhang et al.;[7a] 844 $\mu mol\,h^{-1}\,g^{-1}$). The photocatalytic activity of the amorphous CNs synthesized in an open system in the temperature range 400–600 °C showed that the highest activity was achieved for the CN synthesized at a reaction temperature of 500 °C (1080 $\mu mol\,h^{-1}\,g^{-1}$); this activity corresponds to an approximately 50% enhancement compared to that of raw melon (see Table 1).

Table 1: Physicochemical properties and photocatalytic activity of different Pt/CN_x species for the hydrogen evolution reaction driven by visible light.

Catalyst	Surface area [$m^2\,g^{-1}$]	C/N molar ratio	Hydrogen evolution rate [$\mu mol\,h^{-1}\,g^{-1}$]	Quantum efficiency [%]
PTI/Li^+Cl^-	37	0.68	864	0.60
Melon	18	0.62	722	0.50
$aPTI_{500°C}$	122	0.69	1080	0.75
$aPTI\_4AP_{16\%}$	60	0.82	4907	3.40

Although the above results show a moderate improvement of the photocatalytic activity of PTI-derived materials compared to melon-based ones, when PTI is doped with 4AP the increase in the photoactivity of PTI is a function of the doping level and synthesis temperature. By increasing the temperature from 400 to 600 °C, an optimum photocatalytic activity was measured for the material synthesized at 550 °C (see the Supporting Information, Figure S13). When the content of 4AP was increased from 2 to 64%, the highest photocatalytic activity of 4907 $\mu mol\,h^{-1}\,g^{-1}$ (3.4% quantum efficiency) was detected for 16% doped aPTI, synthesized at 550 °C ($aPTI\_4AP_{16\%}$; Figure S14 in the Supporting Information and Table 1). In essence, the photocatalytic activity of PTI/Li^+Cl^- can be enhanced by 5–6 times upon doping with 4AP in a simple one-pot reaction. 4AP doping of crystalline PTI/Li^+Cl^- leads to no apparent photocatalytic activity. Also, as a control experiment, pure 4AP was shown to be photocatalytically inactive by itself and under ionothermal or thermal treatment. Water oxidation experiments in which O_2 evolution was measured, carried out in the presence of a Co_3O_4 co-catalyst, did not yield substantial amounts of oxygen, thus suggesting that either water oxidation is thermodynamically unfeasible or that the reaction conditions need to be further optimized.

A typical TEM micrograph shows that the surface morphology of doped aPTI is layered and platelet-like

(Figure 2d and S11 in the Supporting Information). The crystallite size and composition of the platinum nanoparticles deposited on the carbon nitride catalyst in situ were studied by TEM and EDX. The results reveal that the photoinduced reduction of the co-catalyst results in well-dispersed nanoparticles roughly 5 nm in diameter.

N_2 sorption measurements allow us to quantify the impact of the surface area (SA) of the catalysts on the photocatalytic activity. In Table 1, the measured specific Brunauer–Emmett–Teller (BET) SAs indicate a weak correlation between SA and activity, but the increased photoactivity in the doped species cannot be rationalized by an increased SA alone.

As seen in Figure 3, the aPTI_4AP$_{16\%}$ photocatalyst yields an orange-brown suspension and its diffuse reflectance spectrum spans across the visible region. It is therefore instructive to examine the wavelength-specific hydrogen production to determine which wavelengths actively contribute to the H_2 evolution. In the wavelength dependence graph (Figure 4), the absorption is overlaid with the wavelength-specific hydrogen evolution. The hydrogen production rate falls off at 450–500 nm, thus indicating that the majority of photons contributing to the hydrogen production are at $\lambda < 500$ nm It is suggested that the active absorption follows the band edge observed between 430 and 440 nm. This band is similar to that seen for the other PTI compounds although red-shifted by the 4AP doping. The broad absorption profile suggests the existence of intra band-gap electronic states at various energies, which could arise from the incorporated 4AP (see the Supporting Information, Figure S4 and S5). However, as Figure 4 infers, not all electronic states—especially those associated with absorption at higher wavelengths—contribute to the hydrogen evolution but may rather act as traps and quenching sites for excitons. We therefore envision that through active control of the number and position of defects in the material, photocatalysts with further enhanced activity can rationally be designed. Nevertheless, the increased visible-light activity up to approximately 500 nm in doped PTI results in a significant improvement over its undoped or crystalline counterparts and is a contributing factor to its high photoactivity.

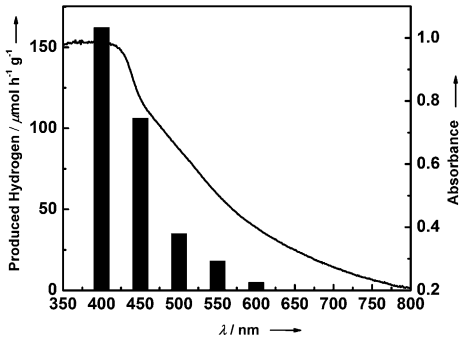

Figure 4. Overlay of UV–Vis spectrum and wavelength-specific hydrogen production (black bars) of aPTI_4AP$_{16\%}$ using 40 nm FWHM band-pass filters.

In conclusion, we have reported a new family of 2D triazine-based carbon nitrides that shows substantial visible-light-induced hydrogen production from water, and in this regard rivals the benchmark heptazine-derived photocatalysts. With external quantum efficiencies as high as 3.4%, the amorphous carbon- and oxygen-enriched poly(triazine imide) species not only outperform melon-type photocatalysts, but also crystalline PTI by 5 to 6 times. Consistent with previous results,[13] we have demonstrated that a rather low level of structural definition and the introduction of defects up to a certain doping level (16% for 4-amino-2,6-dihydroxypyrimidine) tend to enhance the photoactivity of the catalysts. We believe that the diverse range of available organic and inorganic dopants will allow the rational design of a broad set of triazine-based CN polymers with controlled functions, thus opening new avenues for the development of light-harvesting semiconductors. The easily adjustable structural and electronic properties of CN polymers render them particularly versatile for solar energy applications.

Received: August 22, 2012
Published online: January 22, 2013

Keywords: carbon nitrides · copolymerization · photocatalysis · triazines · water splitting

[1] X. Chen, S. Shen, L. Guo, S. S. Mao, *Chem. Rev.* **2010**, *110*, 6503–6570.
[2] H. Tong, S. Ouyang, Y. Bi, N. Umezawa, M. Oshikiri, J. Ye, *Adv. Mater.* **2012**, *24*, 229–251.
[3] a) X. Wang, K. Maeda, A. Thomas, K. Takanabe, G. Xin, J. M. Carlsson, K. Domen, M. Antonietti, *Nat. Mater.* **2009**, *8*, 76–80; b) E. Kroke, M. Schwarz, E. Horath-Bordon, P. Kroll, B. Noll, A. D. Norman, *New J. Chem.* **2002**, *26*, 508–512.
[4] a) Y. Wang, X. Wang, M. Antonietti, *Angew. Chem.* **2012**, *124*, 70–92; *Angew. Chem. Int. Ed.* **2012**, *51*, 68–89; b) Y. Zheng, J. Liu, J. Liang, M. Jaroniec, S. Z. Qiao, *Energy Environ. Sci.* **2012**, *5*, 6717–6731.
[5] a) B. V. Lotsch, M. Döblinger, J. Sehnert, L. Seyfarth, J. Senker, O. Oeckler, W. Schnick, *Chem. Eur. J.* **2007**, *13*, 4969–4980; b) L. Seyfarth, J. Seyfarth, B. V. Lotsch, W. Schnick, J. Senker, *Phys. Chem. Chem. Phys.* **2010**, *12*, 2227–2237; c) B. Jürgens, E. Irran, J. Senker, P. Kroll, H. Müller, W. Schnick, *J. Am. Chem. Soc.* **2003**, *125*, 10288–10300.
[6] a) D. Mitoraj, H. Kisch, *Chem. Eur. J.* **2010**, *16*, 261–269; b) E. Kroke, M. Schwarz, *Coord. Chem. Rev.* **2004**, *248*, 493–532; c) G. Goglio, D. Foy, G. Demazeau, *Mater. Sci. Eng. R* **2008**, *58*, 195–227; d) X. Li, J. Zhang, L. Shen, Y. Ma, W. Lei, Q. Cui, G. Zou, *Appl. Phys. A* **2009**, *94*, 387–392.
[7] a) J. Zhang, X. Chen, K. Takanabe, K. Maeda, K. Domen, J. D. Epping, X. Fu, M. Antonietti, X. Wang, *Angew. Chem.* **2010**, *122*, 451–454; *Angew. Chem. Int. Ed.* **2010**, *49*, 441–444; b) Q. Li, B. Yue, H. Iwai, T. Kako, J. Ye, *J. Phys. Chem. C* **2010**, *114*, 4100–4105; c) Y. Zhang, A. Thomas, M. Antonietti, X. Wang, *J. Am. Chem. Soc.* **2009**, *131*, 50–51; d) H. Yan, Y. Huang, *Chem. Commun.* **2011**, *47*, 4168–4170.
[8] E. Wirnhier, M. Döblinger, D. Gunzelmann, J. Senker, B. V. Lotsch, W. Schnick, *Chem. Eur. J.* **2011**, *17*, 3213–3221.
[9] M. J. Bojdys, J.-O. Müller, M. Antonietti, A. Thomas, *Chem. Eur. J.* **2008**, *14*, 8177–8182.
[10] a) B. V. Lotsch, W. Schnick, *Chem. Mater.* **2006**, *18*, 1891–1900; b) A. I. Finkel'shtein, *Opt. Spektrosk.* **1959**, *6*, 33; c) M. Takimoto, *Kogyo Kagaku Zasshi* **1961**, *64*, 1452–1454; d) M.

Takimoto, *Nippon Kagaku Zasshi* **1964**, *85*, 159 – 168; e) D. A. Long, *J. Raman Spectrosc.* **2004**, *35*, 905 – 905; f) B. V. Lotsch, W. Schnick, *Chem. Eur. J.* **2007**, *13*, 4956 – 4968.

[11] a) P. Niu, G. Liu, H.-M. Cheng, *J. Phys. Chem. C* **2012**, *116*, 11013 – 11018; b) A. Thomas, A. Fischer, F. Goettmann, M. Antonietti, J.-O. Müller, R. Schlögl, J. M. Carlsson, *J. Mater. Chem.* **2008**, *18*, 4893 – 4908; c) A. V. Semencha, L. N. Blinov, *Glass Phys. Chem.* **2010**, *36*, 199 – 208; d) X. Q. Gong, A. Selloni, M. Batzill, U. Diebold, *Nat. Mater.* **2006**, *5*, 665 – 670; e) M. K. Nowotny, L. R. Sheppard, T. Bak, J. Nowotny, *J. Phys. Chem. C* **2008**, *112*, 5275 – 5300.

[12] a) X. Wu, K. W. Zilm, *J. Magn. Reson. Ser. A* **1993**, *102*, 205 – 213; b) C. Gervais, F. Babonneau, J. Maquet, C. Bonhomme, D. Massiot, E. Framery, M. Vaultier, *Magn. Reson. Chem.* **1998**, *36*, 407 – 414.

[13] a) X. Chen, L. Liu, P. Y. Yu, S. S. Mao, *Science* **2011**, *331*, 746 – 750; b) M. Alvaro, E. Carbonell, V. Fornés, H. García, *ChemPhysChem* **2006**, *7*, 200 – 205; c) G. Zhang, J. Zhang, M. Zhang, X. Wang, *J. Mater. Chem.* **2012**, *22*, 8083 – 8091.

[14] While this paper was in review, complementary data on the photocatalytic water splitting of crystalline PTI were published: Y. Ham, K. Maeda, D. Cha, K. Takanabe, K. Domen, *Chem. Asian J.* **2013**, *8*, 218–224.

